Turunen, Konsta; Mikkola, Valtteri; Laukkanen, Timo; Seppälä, Ari

Long-term thermal energy storage prototype of cold-crystallizing erythritol-polyelectrolyte

Published in:
Applied Energy

DOI:
10.1016/j.apenergy.2022.120530

Published: 15/02/2023

Document Version
Publisher's PDF, also known as Version of record

Please cite the original version:
Turunen, K., Mikkola, V., Laukkanen, T., & Seppälä, A. (2023). Long-term thermal energy storage prototype of cold-crystallizing erythritol-polyelectrolyte. *Applied Energy*, *332*, Article 120530.
https://doi.org/10.1016/j.apenergy.2022.120530

Applied Energy 332 (2023) 120530

Contents lists available at ScienceDirect

Applied Energy

journal homepage: www.elsevier.com/locate/apenergy

Long-term thermal energy storage prototype of cold-crystallizing erythritol-polyelectrolyte

Konsta Turunen[a,*], Valtteri Mikkola[b], Timo Laukkanen[a], Ari Seppälä[a]

[a] *Department of Mechanical Engineering, School of Engineering, Aalto University, P.O. Box 16100, 00076 Aalto, Finland*
[b] *Fincoil Lu-Ve Group, R&D, Ansatie 3, 01740 Vantaa, Finland*

HIGHLIGHTS

- Demonstrating supercooling and cold-crystallizing TES of two months at 6.5 kg scale.
- Melting and cold-crystallization enthalpy of ~ 166 J/g and ~ 140 J/g in the prototype.
- Overall efficiency of 0.50–0.80 with combined short- and long-term storage.
- Critical cooling rate predicts spontaneous crystallization on supercooling.
- No undesired crystallization during storage stage with metallic heat exchangers.

ARTICLE INFO

Keywords:
Thermal energy storage
Phase change material
Prototype
Supercooling
Cold crystallization
Experimental

ABSTRACT

Phase change materials can improve the energy density of thermal energy storages (TES) by using the latent heat of melting, but they cannot typically operate efficiently in long-term TES. A unique way to store the latent heat for long-term can be achieved with erythritol-polyelectrolyte mixture, which exploits supercooling, glass transition and cold-crystallization in the storing process. However, the main challenge of supercooling TES is to prevent premature crystallization during supercooling while maintaining adequate heat release rate at large scale. This work determines, for the first time, the key operational parameters of using ~ 6.5 kg of an erythritol-polyelectrolyte mixture in a long-term TES prototype. The prototype yielded an average melting enthalpy of ~ 166 J/g for the mixture which was corroborated with calorimetric measurements. Results confirmed operational feasibility of the prototype TES with an overall storage efficiency of 0.50–0.80 when the latent heat of melting is used for long-term storage and the sensible heat of supercooling for short-term storage. The prototype enabled determination of previously undefined critical cooling rate, above which premature crystallization during supercooling was not observed despite the stochastic nature of supercooling and crystallization. Furthermore, momentary heat release rate of 1000 W was achieved by allowing complete cold-crystallization before discharging the heat. The operational parameters defined in this work confirm reliable use of cold-crystallization in long-term TES at kilogram scale with realistic operational values which forwards the implementation of advanced cold-crystallizing materials in long-term TES applications.

1. Introduction

Thermal energy storages (TES) can be used to balance the variability of renewable energy generation and consumption by releasing the stored energy as heat. They are typically categorized in three groups by the way thermal energy is stored. First, sensible heat storages rely on increasing and decreasing the temperature of a storage medium, such as water. Second, latent heat storages utilize the heat involved in phase transition, for example melting and crystallization of a material. Lastly, chemical reactions store thermal energy in reversible reactions, for example water vapor sorption on material surface.

Latent heat storages are useful, because they can store large amount of thermal energy at a narrow temperature range via phase change. Typically, phase change material (PCM) crystallizes as it cools below the melting temperature. However, if PCM remains in a liquid state below the melting temperature, it supercools. Supercooling is undesirable in

---

* Corresponding author.
E-mail address: konsta.turunen@aalto.fi (K. Turunen).

https://doi.org/10.1016/j.apenergy.2022.120530
Received 6 July 2022; Received in revised form 10 November 2022; Accepted 14 December 2022

conventional short-term TES, because it delays the heat release [1,2]. Nevertheless, supercooling can be advantageous in long-term TES: If PCM remains supercooled, i.e. in a metastable state, the latent heat of melting can be stored without loss indefinitely.

At small scale, supercooling TES has been applied commercially in re-usable heating pads, where supercooling sodium acetate trihydrate (SAT) stores thermal energy [3]. However, spontaneous crystallization during the supercooling inflicts the main challenge of implementing supercooled TES at large scale. For example, when SAT storage was scaled-up to 100–200 kg size, premature crystallization was observed during supercooling in several researches listed in [4]. Factors such as, rough surfaces, pressure changes, mechanical stress and impurities may initiate crystallization prematurely [1,5]. Moreover, as the size of the PCM unit increases, the probability of nucleation increases in the supercooled state, because crystallization is a stochastic phenomenon [6,7]. Usually, additives, such as extra water, carboxymethyl cellulose or xanthan gum, are mixed with SAT, to reduce phase separation and spontaneous nucleation, but this reduces the melting enthalpy from 260 J/g typically to 160–240 J/g [8] and it cannot yet guarantee reliable supercooling TES at large scale applications. Supercooled TES has been also analysed with several other salt hydrates such as, calcium chlorite pentahydrate [9], sodium thiosulfate pentahydrate (STP) [10], disodium hydrogen phosphate dodecahydrate [3], and mixtures of SAT and STP [11]. However, they face the same challenges as SAT. Similarly, solid–solid phase transitions can store thermal energy in a metastable state, as demonstrated in milligram scale by lambda-trititanium pentoxide, which can store a latent heat of 230 MJ/m^3 and release it by applying pressure of 60 MPa [12].

Sugar alcohols also exhibit high melting enthalpy and large supercooling degree, which is defined as the temperature difference between the melting and supercooled material temperature ($T_m - T$). Most sugar alcohols, such as erythritol and mannitol, cannot reliably store thermal energy in the supercooled state, because of the spontaneous crystallization. Nevertheless, supercooling stability of erythritol can be improved by reducing the sample size and confining the material, for example into micro- or nanoscale pores [13,14]. Supercooling stability can be also improved by maintaining low supercooling degree. For example, 0.9-liter tubes of threitol remained in the supercooled state for three days at a supercooling degree of 18 °C ($T_m = 87$ °C), which was maintained with a heater [15]. However, threitol experienced crystallization inside the tubes when the supercooling degree was increased over 18 °C. Despite these efforts, research is still required to implement reliable and long-term applications at large scale. On the other hand, sugar alcohols that show sufficient stability of the supercooled state in small sample size, such as xylitol and eutectic mixtures of polyols, exhibit slow crystallization and heat release rates [16,17]. This has prevented their efficient use in real-life applications, but development on improving their crystallization rate is still ongoing [17–19].

Scaling-up PCMs from small sample sizes to prototype and pilot systems may result in worse operational behaviour than expected [20–22]. For instance, numerical analysis conducted by idealized thermal properties rarely reflect the reality in large-scale applications which can cause, e.g., lower energy storage densities than indicated by the material properties [20]. This can also be manifested as varying values of melting enthalpy and as a melting temperature range [23]. Furthermore, insufficient attention to the material characteristics may result in undesirable operation in large-scale applications: PCM may solidify to another crystal structure than the thermodynamically stable structure (polymorphism) which impairs the reliability and storage capacity of TES. This is a challenge for sugar alcohols, as they exhibit varying values of melting enthalpy and temperature, which is characteristic for polymorphism [16,24–26]. Incongruent melting and phase separation also decrease the energy density and reliability of the storage, which has been exemplified by salt hydrates, such as SAT [27,28]. Moreover, use of supercooling TES complicates scaling-up, as discussed in previous paragraphs. This could cause scarcity of the scaling up attempts of supercooling TES in the literature.

Mixtures of sugar alcohols and polymers have demonstrated adequate heat release rates, a simple method for triggering heat release and sufficient stability of supercooling for long-term TES at milligram and gram scale [29–32]. This class of materials utilizes glass transition and cold-crystallization to store and release thermal energy, as illustrated in Fig. 1. First, the storage is charged by melting the material. Next, the material is supercooled close to the glass transition temperature, where kinetics slows down significantly. This ensures reliable storage, because even if crystallization begins, crystal growth is so slow that the latent heat can be stored for several months without reduction [30]. The heat release is triggered by re-heating the material to the cold-crystallization temperature (T_{cc}) which increases the molecular movement to the extent that the material crystallizes, i.e., cold-crystallization occurs. Crystallization releases heat, which increases the material temperature towards the melting temperature. Thus, the storage can be discharged. Among cold-crystallizing materials, erythritol in a cross-linked sodium polyacrylate (CCM) has previously shown feasible operation in 160-g scale [30], and predictable crystallization kinetics in milligram scale [32]. In these two studies, premature crystallization was not observed during the supercooling stage. However, CCM has not yet been scaled up to a larger size or tested in applications.

As above literature indicates, large-scale supercooling TES must overcome the barrier of unreliable supercooling, while maintaining an adequate crystallization and heat release rates. This necessitates a detailed analysis of the material behaviour and properties using large sample sizes and an evaluation of the operational TES parameters in a prototype system before a new supercooling PCM can be reliably employed for TES use.

In this work, cold-crystallizing TES material (CCM) is for the first time scaled up to a kilogram scale and its operational parameters are established in a long-term TES prototype using complete storage cycles. The prototype confirmed operational feasibility of CCM in two types of heat transfer arrangements (finned-tube and shell-and-closed-tube heat exchangers), which yielded similar melting enthalpy (~166 J/g) as in DSC (178 J/g). The analysis of each stage of the storage cycle (see Fig. 1) revealed a maximum storage efficiency of 0.50–0.80, which depends on the discharging temperature level and the utilizable sensible heat during supercooling. Moreover, we determined previously undefined parameter, critical cooling rate, which can be used to estimate the occurrence of premature crystallization during supercooling. This work presents essential parameters for designing and predicting the behaviour of CCM in large-scale supercooled TES applications.

2. Materials and methods

2.1. Material preparation

Preparation of erythritol in cross-linked sodium acrylate (CCM) follows a method developed and described in detail in our previous work [29]. In short, sodium hydroxide (assay ≥ 99 %, VWR Chemicals), acrylic acid (assay ≥ 99 %, Merck) and ethylene glycol dimethacrylate (assay ≥ 97.5 %, Merck), were mixed in aqueous erythritol (Food grade, Suomen Luontaistukku ltd., Finland), which had mass ratio of $W_{Ery}/W_{H2O} = 1.5$. After thorough mixing, potassium persulfate (assay ≥ 98 %, VWR Chemicals), was added to initiate polymerization of sodium polyacrylate. Lastly, water was evaporated in an oven at 130 °C. We prepared CCM composition with 80 wt% of erythritol, 17.9 wt% of sodium polyacrylate (100 % molar neutralization degree), 2 wt% of ethylene glycol dimethacrylate and 0.1 wt% of potassium persulfate, as it has previously shown long-term storage ability and sufficient crystallization rate for discharge in 160-g scale [30]. The material was prepared in six batches, from which three batches were used for storage Unit 1 and three for Unit 2.

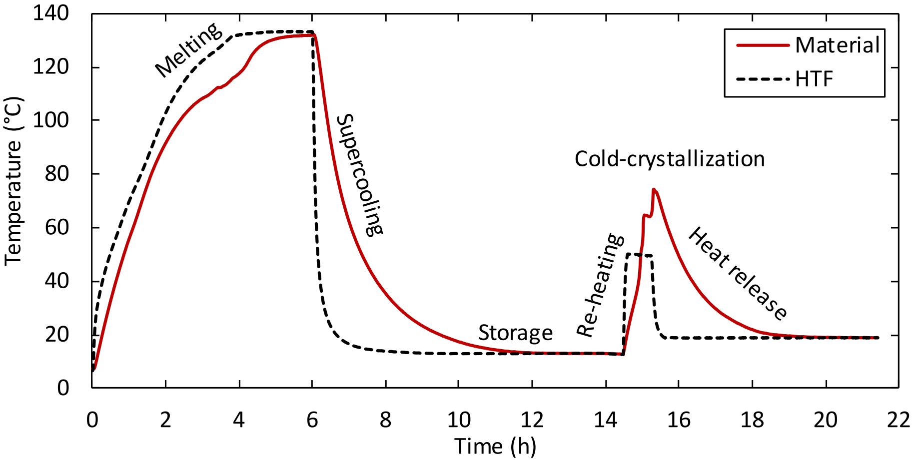

Fig. 1. An example of the temperature development of the material that utilizes glass transition and cold-crystallization for TES. Heat transfer fluid (HTF) heats and cools the material.

2.2. *Thermophysical properties*

Thermal properties of CCM were measured using differential scanning calorimetry (Netzsch DSC204F1 Phoenix DSC). Because CCM was prepared in six separate batches, we collected and measured one DSC sample from each batch. Measurement program consisted of three consecutive heating–cooling cycles from −60 °C to 130 °C with a 5 °C/min scan rate. DSC samples weighted 25 ± 5 mg.

In addition, liquid phase density was measured, because CCM supercools 100 °C below the melting temperature. Solid phase density of CCM was reported in our previous work [30]. The density of CCM and silicon oil was measured using 100 ml and 250 ml measuring glass which have accuracy of ± 0.1 ml and ± 0.2 ml, respectively. The sample masses were 110 g for CCM and 235 g for silicon oil. Temperature controlled chamber stabilized the temperature of the liquids at the desired level, after which the liquid surface level was inspected. Sample masses were weighted before and after the surface level inspection using Precisa 3100C with readability of 0.01 g. Measurements were repeated at least three times for each temperature.

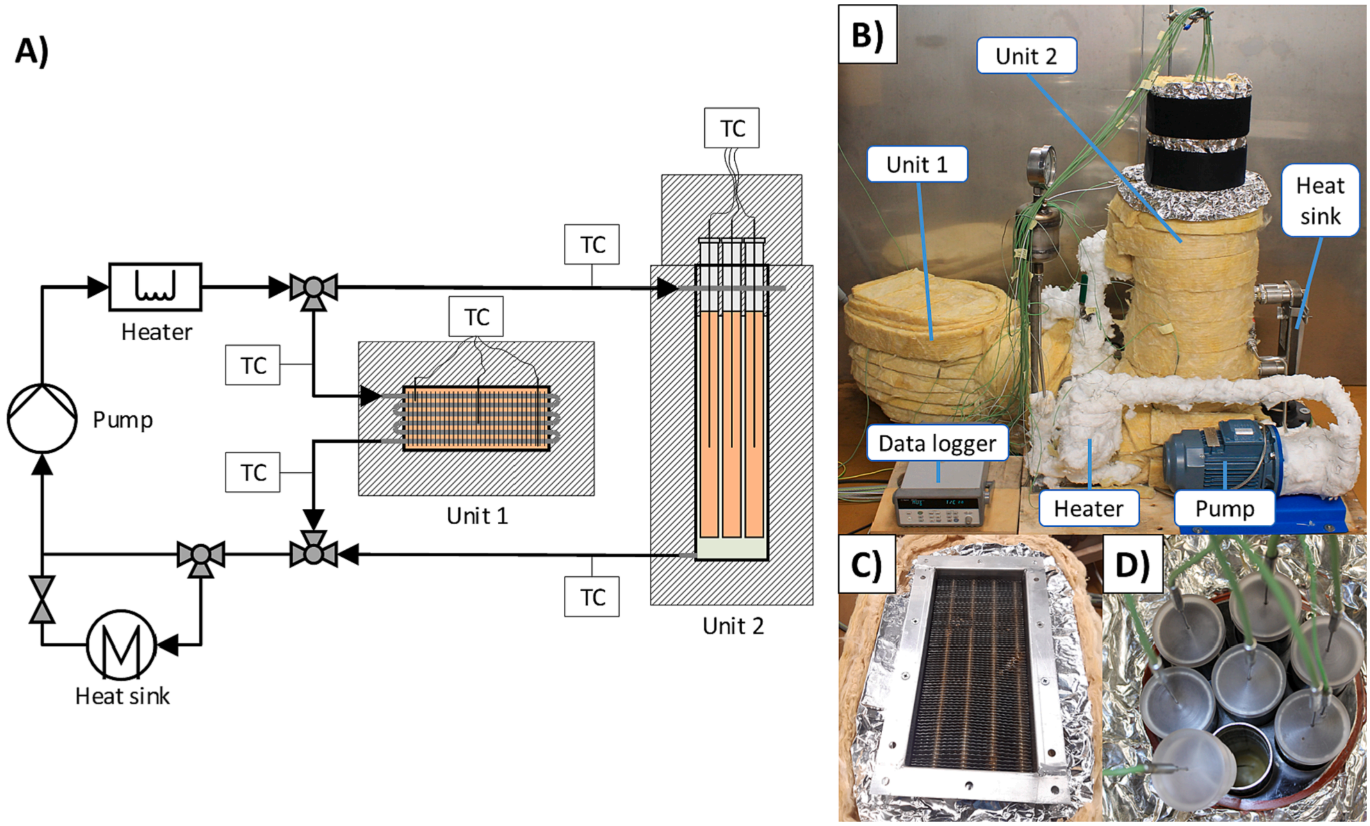

Fig. 2. A) Schematic of the experimental setup, where "TC" indicates a location of a thermocouple. Storage unit 2 contains seven tubes. B) Image of the insulated setup in a refrigeration chamber. C) The fin and tube heat exchanger in Unit 2 after the container was filled with CCM, hence TCs are not visible. D) The shell and closed tube heat exchanger arrangement in Unit 2 imaged from the top. Tubes extended over the top of the container tank enabling visual examination of CCM inside the tubes.

2.3. Experimental setup

Operational principle of CCM has been confirmed in milligram and gram scale [30]. Therefore, a prototype TES system was built in a laboratory to determine operational parameters of CCM in kilogram scale. The system comprises two storage units for analysing operational parameters in different heat transfer arrangements, as depicted in the schematic in Fig. 2A-B. Furthermore, the design of Unit 1 enabled examination of cold-crystallization behaviour and Unit 2 analysation of supercooling stability. The main dimensions of the storage units are summarized in Table 1.

Unit 1 was designed and manufactured by Fincoil Lu-Ve group to ensure adequate heat transfer in the unit, because CCM has relatively low thermal conductivity of 0.77 W/m·K and 0.35 W/m·K in the solid and liquid state [30]. Consequently, Unit 1 employs a typical fin and tube heat exchanger coil, which consists of 16 copper tubes and 79 aluminium fins enclosed inside a rectangular container made of aluminium plates. This way, the total heat transfer surface area of approximately 2.5 m^2 was achieved. Similar fin and tube heat exchanger coils are generally used for air heat exchangers which enables solving the heat transfer problem of CCM by using existing technology. CCM was placed on the fin side where it filled the space between the fins and the tubes (Fig. 2C). All parts of CCM have less than 2 mm distance to the nearest fin which minimizes the length for thermal conduction within CCM and ensures efficient heat transfer. The container was filled approximately to the height of the upper edge of the fins, resulting in total CCM mass of 6.72 kg. The volumetric ratio of CCM to container (V_{CCM}/V_{cont}) was approximately 0.68 for Unit 1. Oil flowed inside the tubes in one flow pass from down to up. The temperature of CCM was measured close to the bottom inlet, mid-point, and top outlet of the container using K-type thermocouples.

Unit 2 was designed to reduce the harmful impact of spontaneous crystallization during cooling from the melting to the storage temperature. It comprised of cylindrical tank, which embodied seven CCM-filled steel tubes, i.e., Unit 2 resembles shell and closed tube heat exchanger. Therefore, if nucleation occurs, crystallization is contained within a single CCM tube leaving the other tubes unaffected. Tubes were filled up to 0.5 m height, resulting in approximately 0.90 kg of CCM in each tube and total CCM mass of 6.31 kg. The tubes extended over the top of the tank which enabled inspection of CCM surface during the operation (Fig. 2D). Oil flowed through six entrance points at the top the tank, to ensure uniform oil flow, while exit located at the bottom of the tank. In addition, K-type thermocouples measured the temperature of CCM at the mid-point of all tubes and at the surface of the material in one tube that located next to the container wall. This way the number of crystallized tubes during cooling can be analysed which indicates the stability during supercooling. The volumetric ratio of CCM to container (V_{CCM}/V_{cont}) was approximately 0.35 for Unit 2. The small ratio for Unit 2 is caused by the seven-tube arrangement and incomplete filling of the tubes, which ensures complete melting of CCM.

The charge of the storage units was controlled with a pump (250 W), which circulated silicon oil (VWR, 10cSt) through one unit at a time. The oil was heated using an electric heater (500 W) and cooled with a heat exchanger connected to the tap water system (Heat sink in Fig. 2A). Oil inlet temperature to the storage units was controlled with a PID-controller, and the oil inlet and outlet temperature was measured with K-type thermocouples. In order to control and maintain the desired temperature of the storage units during the storage period, the setup was constructed inside a refrigeration chamber.

Table 1
The main dimensions of Unit 1, Unit 2 and CCM filled tubes in Unit 2.

Property	Unit 1	Unit 2 tank	Unit 2 tubes
Container shape	Rectangular	Cylindrical	Cylindrical
Container material	Aluminium	Steel	Steel
Wall thickness [m]	0.001	0.002	0.001
Height [m]	0.150	0.70	0.70
Width/diameter [m]	0.315	0.154	0.042
Depth [m]	0.150		
Insulation material	Glass wool	Glass wool	
Insulation thickness [m]	0.1	0.1	
CCM mass [kg]	6.72	6.31	
$V_{CCM}/V_{cont.}$ [-]	0.68	0.35	

2.4. Measurement procedure

Use of CCM for TES consists of five stages: charging (melting by heating), cooling to storage temperature (supercooling), storage, reheating to cold-crystallization temperature and discharging (cold-crystallization). This operational principle is depicted in Fig. 1. The stages were analysed by defining energy balance for the storage unit, as expressed in Eq. (1), where q is heat flux (W) and subscript *sto* refers to storage, *in* to oil inlet, *out* to oil outlet and *loss* to heat loss from the storage to ambient. Because the volumetric flow rate of the heat transfer oil remains constant at the inlet and outlet, a change in enthalpy of the storage unit, ΔH_{sto} (J), in a time step Δt can be approximated as Eq. (2). Consequently, enthalpy-temperature graph (h,T-graph) can be formed, by plotting the cumulative storage enthalpy as a function of CCM temperature, as described in Eq. (3), where H_0 is the reference point of the enthalpy at the temperature where measurement begins and ΔH_{sto}^k a change in enthalpy of the storage at a time step k. T_{CCM} is the average temperature of CCM in the storage.

$$q_{sto} = q_{in} + q_{out} - q_{loss} \tag{1}$$

$$\Delta H_{sto} = \dot{V}\left(\rho_{in} C_{p,in} T_{in} - \rho_{out} C_{p,out} T_{out}\right)\Delta t - q_{loss}\Delta t \tag{2}$$

$$H(T_{CCM}) = H_0 + \sum_{k=1}^{N} \Delta H_{sto}^k \tag{3}$$

Time step of $\Delta t = 30$ s was used throughout this work. The heat loss term was estimated by maintaining a constant oil flow through the storage unit when phase change was not occurring. The measurement continued until the inlet flow, outlet flow and CCM temperatures reached a constant level. The mass flow rate of oil was assumed to be constant, because the change in the oil density at the inlet and outlet was small. In this steady state situation, $\Delta H_{sto} = 0$, which enables calculation of q_{loss} using Eq. (2). Fig. 3 illustrates the determined heat losses for the storage units. The heat losses were calculated as a function of the temperature difference of the storage unit and the ambient, as shown in Fig. 3.

Uncertainty of the measurements was estimated according to the guide by JCGM [33]. Table 2 summarizes the relative expanded uncertainties with 95 % confidence level. We assumed normal distribution for all other measurands than mass, which used rectangular distribution. The volumetric flow rate was controlled with a frequency converter, which was calibrated for different frequencies by measuring the mass of the pumped oil in a time period of approximately 60 s. Temperature showed expanded uncertainty of 0.06 °C using 95 % confidence level.

3. Results and discussion

3.1. Thermophysical properties

Melting and cold-crystallization properties were measured using DSC and the prototype system (Unit 1 and Unit 2). DSC measurements were conducted with six samples which resulted in 14 melting-cold-crystallization cycles. Results of these DSC measurements are listed in Table 3, and a typical DSC measurement is depicted in Fig. 4. The properties show small standard deviations which indicates a consistent preparation method of CCM. The small deviations are mainly caused by the measurement accuracy and stochastic nature of the cold-

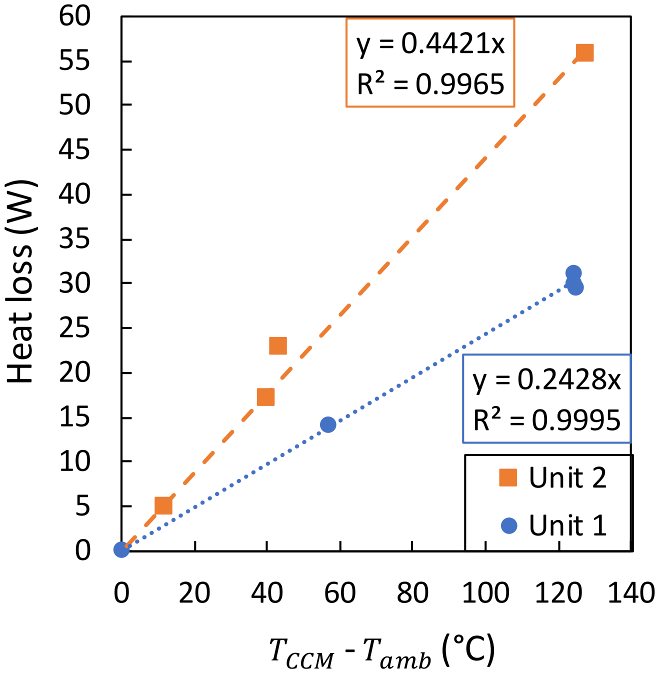

Fig. 3. Heat loss curves for Unit 1 and Unit 2. The equations display the linear fits for the measured points.

Table 2
Relative expanded uncertainties of estimates with 95 % confidence level.

	$\dot{V}$(%)	$C_{p,oil}$(%)	ρ_{oil}(%)	Δt(%)
Expanded uncertainty	2.2	5.5	0.13	0.66

Table 3
Thermophysical properties of CCM with standard deviation. Subscript *g* refers to glass transition, *cc* to cold-crystallization and *m* to melting.

	DSC		Unit 1		Unit 2	
T_g(°C)	−24.7	2.1				
T_{cc}(°C)	55.6	2.8	54.7	1.1	54.8	2.1
ΔH_{cc}(J/g)	130.2	6.7	128.6	1.9	158.3	8.9
T_m(°C)	111.1	1.0	112.0	0.6	110.7	2.4
ΔH_m(J/g)	177.9	3.2	153.0	13.0	179.6	6.0

crystallization of CCM. Comparison between the results from the prototype and DSC is not straightforward. Cold-crystallization properties are influenced by the cooling and heating rates. Furthermore, cold-crystallization temperature (T_{cc}) impacts the cold-crystallization enthalpy (ΔH_{cc}) as formulated in Eq. (4), which defines the enthalpy of crystallization, when the phase change begins in the supercooled state. Therefore, for Unit 1 and Unit 2, Table 3 lists an average value of ΔH_{cc} from three measurements, which yielded approximately the same T_{cc} as DSC measurements.

$$\Delta H_{cc}(T_{cc}) = \Delta H_m(T_m) - \int_{T_{cc}}^{T_m} (C_{p,l} - C_{p,s})dT \tag{4}$$

Table 3 shows that Unit 1 yields lower melting enthalpy (ΔH_m) than DSC, while Unit 2 higher cold-crystallization enthalpy than DSC. These differences most likely stem from the measurement accuracy and the large scale of the experimental setup. Furthermore, the cooling end temperature differs between the DSC (-60 °C) and experimental setup (4–7 °C) which can increase deviations in the kinetics of cold-crystallization. Because of the above-mentioned sources of inaccuracies, moderate deviations between DSC and the experimental setup are expected. Therefore, the results in Table 3 indicate that CCM maintains similar thermal properties in the prototype system as in DSC measurements.

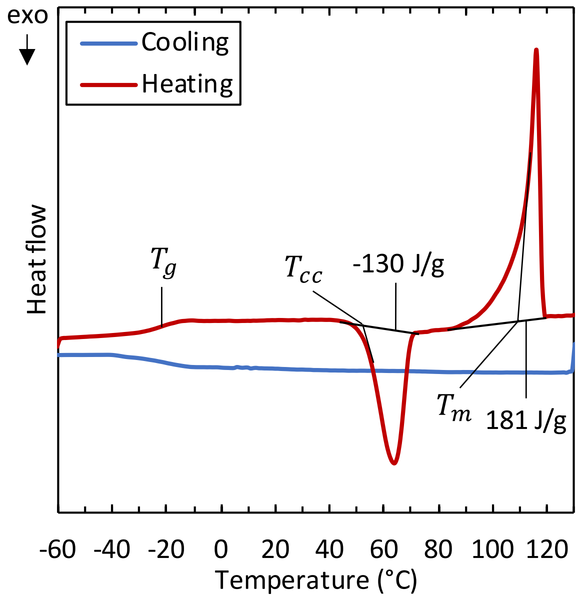

Fig. 4. Typical cooling-heating cycle of CCM measured by DSC.

Liquid density of melt and supercooled CCM was measured as a function of temperature. Density behaves as expected; it increases as the temperature decreases, as displayed in Fig. 5. Furthermore, results correspond to the previous measurements at 25 °C [30]. In the operational range from 0 °C (storage temperature) to 120 °C (melt), density changes approximately 120 kg/m^3. This should be considered in the design of practical applications, as expansion and contraction of CCM can cause malfunction e.g., stress in the equipment. Because crystallization of CCM might begin in the supercooled state, density measurements that showed crystals in the visual inspection were neglected. Using the melting properties measured in DSC, the volumetric melting enthalpy (or energy density) of CCM results in 243 MJ/m^3. It is in the mid-range of typical PCMs used in short-term TES at the corresponding

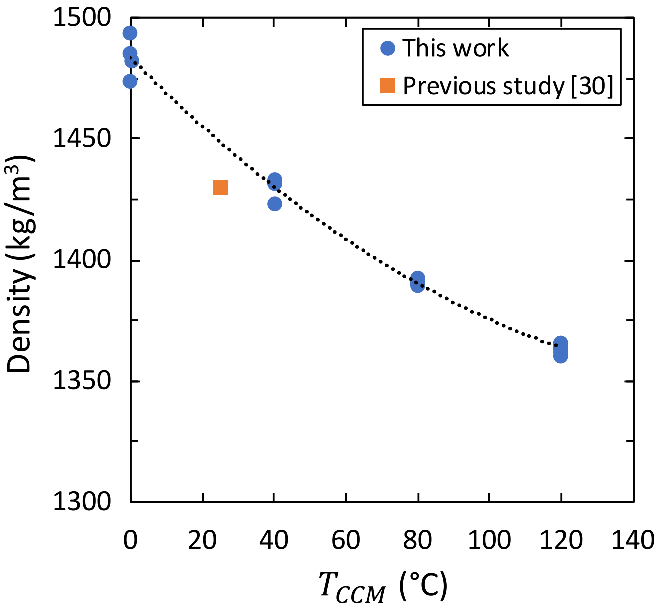

Fig. 5. Liquid density of CCM with an exponential fit (this work), and a value reported in our previous study [30].

temperature [22,34], and comparable to supercooling SAT with additives (200–310 MJ/m^3) [8].

3.2. Charging – melting

The charging measurements aimed to determine an adequate charging temperature, which ensures complete melting of CCM within a reasonable timescale. The highest charging temperature is limited by the evaporation and thermal degradation of CCM, which begin approximately at 150 °C [32]. Thus, storage units were charged by heating CCM to a charging temperature, which ranged from 120 °C to 135 °C, to maintain long-term thermal stability of CCM. The heating was applied with an oil circulation that flowed through an electrical heater (500 W). Unit 1 and Unit 2 showed similar charging rates (q_{sto}) from 150 W to 250 W during heating CCM from the ambient to the melting temperature, as shown in Fig. 6. The charging rate remained similar because electric heater was limiting the charging rate. After CCM melted, the charging rate decreased, as the supply oil temperature reached a constant pre-set value. Because Unit 1 and Unit 2 showed similar charging rates, Fig. 6 exemplifies the charging rate for different supply oil temperatures in Unit 1. As expected, high charging temperature resulted in high charging rate after the melting, which expedites the charging process. For complete melting of CCM, the charging time ranged from 5 h to 6 h for Unit 1 and 6 h to 7 h for Unit 2. When charging time was below these ranges, crystallization was induced on the following cooling. This indicates that small part of CCM was not completely melted, even if the average temperature of CCM reached 120 °C. Especially, Unit 2 showed crystallized areas at the top surface of CCM after melting was observed by thermocouples. The top section of CCM tubes melted more slowly than the bottom section probably because the CCM tubes extended over the top of the tank, increasing heat losses at the top of the tubes. Therefore, Unit 2 required longer charging time than Unit 1. These results emphasize vulnerability of the charging process: The storage system ought to be carefully designed to ensure complete melting of CCM, as even small crystal fraction can prematurely crystallize CCM during cooling to storage temperature. For example, if an optimal one-day charging was desired, capacity of a single storage unit should not exceed the amount of chargeable solar energy during daytime, because it would result in incomplete melting.

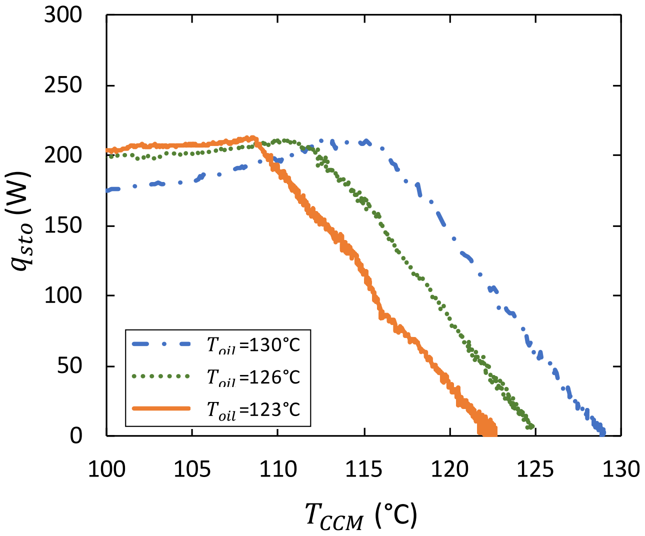

Fig. 6. Charging rate of Unit 1 with different setting values of the oil inlet temperature (T_{oil}). The oil inlet temperature reached the set value only after the most of CCM was melted. Therefore, the charging rate remained similar in the measurements untilT_{CCM} = 110–115 °C, and the impact of the oil temperature on the charging rate emerged at higher temperatures.

3.3. Critical cooling rate

So far, crystallization of CCM on cooling has not been observed in controlled measurements using DSC with cooling rate of 0.5 °C/min or above [32] or 160-g glass bottles with free convection cooling to 0 °C [30]. CCM's stability against crystallization on cooling from the melting to the storage temperature determines the functionality of the long-term storage. Therefore, the slowest cooling rate without crystallization, i.e., critical cooling rate, is a key parameter for viable TES use. Unit 2 contains seven CCM tubes, which can be used to analyse crystallization on cooling. Premature crystallization was observed by measuring temperature at the midpoint of the tubes and by visual inspection of the top surface of CCM at the end of cooling. Additionally, temperature of CCM's surface was measured in a tube that was located next to the container wall.

Fig. 7B illustrates the average cooling rate of CCM in Unit 2, when Fast, Semi-slow and Slow cooling modes were used. The cooling rate decreases linearly as CCM temperature reduces, because the cooling capacity of the heat sink depends on the incoming oil temperature. Fast cooling mode induced no crystallization, when charging temperature was set to 130–135 °C and time was maintained above 390 min. Slow cooling mode was repeated four times, resulting in total of 28 cooling events per tube. Temperature sensors recorded one complete crystallization of a tube, which is shown as a peak in the cooling rate at 53 °C in Fig. 7B. After the storage temperature was achieved, visual inspection revealed that crystallization was initiated at the CCM-air surface in some of the tubes in Slow cooling mode measurements, as shown in Fig. 8A. Temperature sensors were unable to record these crystallizations, because crystallization remained at the top section of the tube. In total, four tubes experienced varying degrees of crystallization at the surface. It is possible that small crystals formed also in the deeper region of CCM, but visual inspection was limited only to a few centimetres' depth from the surface. Nevertheless, crystal fraction remained low, as released heat in the cold-crystallization for all four measurements ranged from 111 J/g to 147 J/g.

As slow cooling mode induced some crystallization, three measurements were conducted also with semi-slow cooling mode. Semi-slow cooling mode begins with cooling rate of 0.5 °C/min gradually reducing to 0.1 °C/min as the material temperature decreases from 100 °C to 20 °C, respectively. Semi-slow cooling mode induced one small crystal with approximately 0.5 cm diameter, which is shown in Fig. 8B, indicating that this mode operates at the critical cooling rate. This is an important finding, as the critical cooling rate can be used to determine the maximum size of a single CCM storage unit without crystallization during supercooling which increases predictability of the storage. Current supercooling TES system have difficulties in avoiding premature nucleation in large scale systems with heat transfer arrangements. For example, SAT storages of 100–200 kg have experienced supercooling success rate ranging from 15 % to 70 % [4]. The above defined critical rate applies for approximately 0.90 kg of CCM in a steel tube container with an air-CCM contact at the top.

To compare, Fig. 7A shows the tested cooling modes for Unit 1. The cooling rate in Unit 1 was 2–4 times higher than compared to Unit 2 because of the enhanced heat transfer arrangement. Consequently, Fast cooling mode indicates no crystallization in any of the measurements. On the other hand, the slow cooling mode induced partial crystallization in two of the three cooling tests. This partial crystallization is illustrated in Fig. 7A, where peak in the cooling rate at 70 °C indicates heat release that slows down the cooling. Moreover, visual examination of the storage unit revealed partial crystallization of CCM, as shown in Fig. 8C. Semi-slow cooling mode induced no evident crystallization in the temperature data or in the visual inspection and it was repeated four times, during which crystallization heat varied from 116 J/g to 125 J/g. Therefore, the critical cooling rate for Unit 1 appears to correspond Semi-slow cooling mode. However, accurate definition of critical cooling rate in Unit 1 is challenging, as crystallization is a stochastic

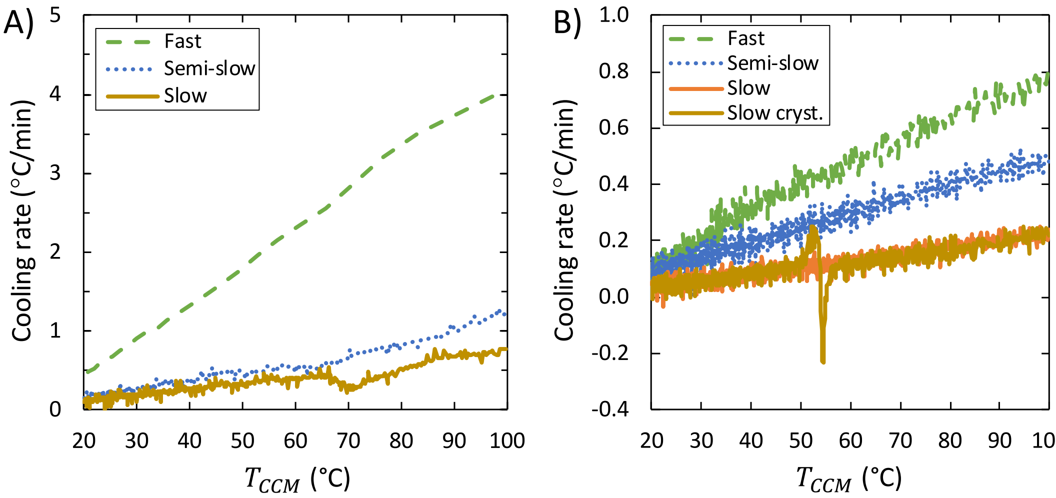

Fig. 7. Cooling rate of CCM using Fast, Semi-slow and Slow cooling rate in Unit 1 (A) and Unit 2 (B). The enhanced heat transfer arrangement in Unit 1 causes faster cooling rates than compared to Unit 2.

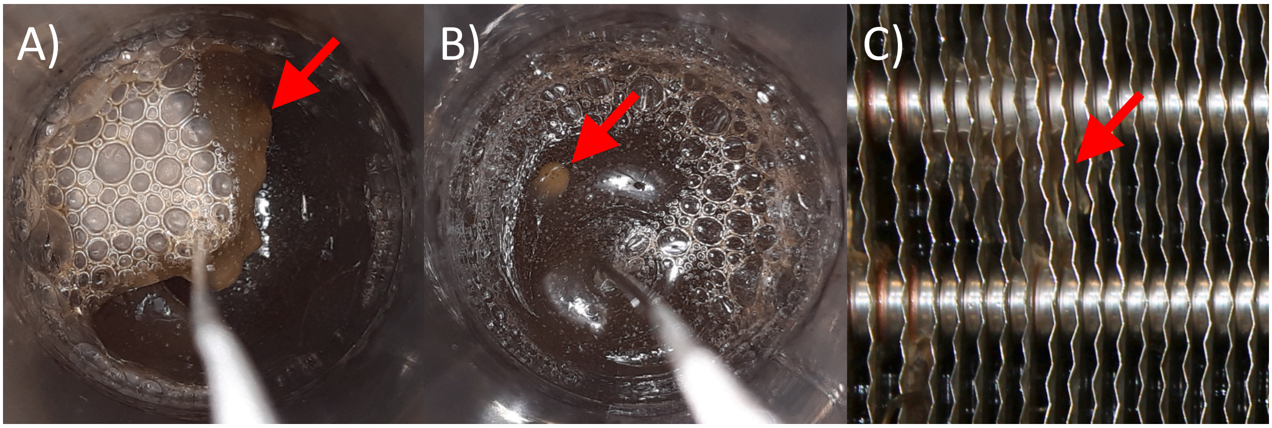

Fig. 8. Partial crystallization at the surface of CCM in Slow cooling mode of Unit 2 (A), small crystal induced in Semi-slow cooling mode of Unit 2 (B), and partial crytallization in Slow cooling mode of Unit 1 (C). Red arrows point to the crystallized area. (For interpretation of the references to colour in this figure legend, the reader is referred to the web version of this article.)

phenomenon and conducting sufficient number of charge–discharge cycles with several cooling rates is time-consuming.

The vulnerable cooling temperature range extends from the melting point to approximately 20 °C, below which crystallization rate of CCM slows down significantly [32]. Semi-slow cooling rate in Unit 2 reduced from 0.5 °C/min to 0.1 °C/min with a temperature decrease from 100 °C to 20 °C, which corresponds to mass-specific cooling rate decrease from 0.6 °C/(kg·min) to 0.1 °C/(kg·min), respectively. In comparison, mass-specific cooling rate of Semi-slow cooling mode in Unit 1 (0.9 °C/(kg·min) and 0.04 °C/(kg·min)) is similar to critical cooling rate in Unit 2 which indicates that the large metal surface in Unit 1 has no significant impact on cooling stability of CCM. This is beneficial, as material surfaces typically induce crystallization via heterogenous nucleation reducing the supercooling ability of the material [6]. The comparison of mass-specific cooling rates is approximate, because of the different heat transfer arrangements in Unit 1 and Unit 2. Nevertheless, even if crystallization was initiated during cooling, CCM did not always crystallize completely. It appears that even slow cooling rates below 0.5 °C/(kg·min) can suppress crystal growth, preventing complete crystallization. Contrarily, after cooling and re-heating, CCM crystallizes quickly increasing the temperature towards melting point. This difference in crystallization rate on cooling and re-heating most likely rises from the peculiar energy landscape of CCM, hence it enables TES use [32].

3.4. *Storage efficiency*

CCM is cooled to the storage temperature to reduce the crystallization rate to the extent that long-term storage can be achieved. In order to evaluate the impact of the storage temperature on the storage ability of CCM, the storage efficiency was determined for storage temperatures of 4 °C and 7 °C. In this work, the storage efficiency is defined as the ratio of the cold-crystallization enthalpies after the storage period, *t* (d), and after 2-day storage ($\Delta H_{cc,t}/\Delta H_{cc,2}$). In other words, the storage efficiency shows the ratio of the stored latent heat that is released. Fig. 9 illustrates the storage efficiency of Unit 1 and Unit 2 for storage temperature of 4 °C and 7 °C. For both units, the storage efficiency at 4 °C remains high for one month, after which it begins to decrease because of slow crystallization. Similar results were observed when 160-g samples of CCM were stored in glass bottles at 5 °C storage temperature [30]. This indicates that the existence of plate heat exchanger (Unit 1) and tubes (Unit 2) does not significantly accelerate the crystallization during the storage. Even the large metal surface area in Unit 1 (2.5 m^2) appears to have negligible impact on the crystallization during the storage period.

When the storage temperature was increased to 7 °C, the efficient storage time reduces to two weeks in Unit 2. This large decrease in the efficiency is caused by a drastic change in kinetics of the supercooled CCM below 1.2 T_g (~25 °C). In our previous work [32], Arrhenius

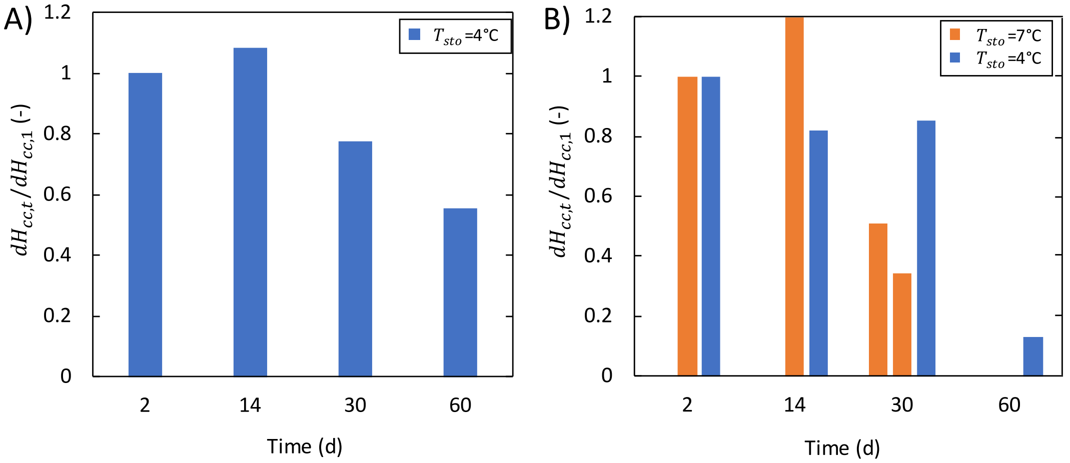

Fig. 9. Storage efficiency of Unit 1 (A) and Unit 2 (B). Efficiency above unity is caused by deviations in measurements. The low value at 60 d (0.15) for Unit 2 is most likely caused by a one-day power outage, which increased the storage temperature before the discharge measurement.

equation correctly predicts the crystallization rate constant at above 10 °C. However, below 10 °C, CCM's crystallization rate constant decreases faster than the Arrhenius equation predicts [32]. Therefore, CCM is sensitive for the changes in the storage temperature. On one hand, a small reduction of storage temperature results in relatively large extension of the efficient storage period. For example, storage efficiency remained high at 0 °C for at least three months in 160-g scale [30]. On the other hand, small increases of the storage temperature can cause accelerated crystallization during the storage. Indeed, the storage efficiency results emphasize the significance of a correct storage temperature. This phenomenon may have also caused the low storage efficiency value at the 60-day storage period in Unit 2 (Fig. 9B), because one-day electricity outage increased the temperature of the storage before the discharge measurement begun. The long-term storage tests at 7 °C were conducted only using Unit 2 because of the time-consuming characteristics of the measurements. If high storage efficiency is desired for longer storage periods without decreasing the storage temperature, the composition of CCM can be adjusted by decreasing the mass fraction of erythritol. However, this will also reduce the energy density of CCM. Impact of the composition on storage efficiency and thermal properties of CCM was analysed in our previous studies [30,32]. The efficient storage temperature of CCM is relatively low compared to the other supercooling TES materials, which are typically maintained at the ambient temperature during the storage. Even though the lower temperature complicates the storage system, it ensures reliable storage, which is essential for a feasible system.

3.5. Re-heating – cold-crystallization temperature

Crystallization behaviour during discharging was analysed using Unit 1, as it comprises from one single unit of CCM. Discharging process of CCM can be divided in three parts: re-heating to cold-crystallization temperature (T_{cc}), cold-crystallization and discharging the heat, as illustrated in Fig. 1. The re-heating determines a response time to demand, as CCM requires heating to the cold-crystallization temperature for self-sustaining and fast crystallization. Therefore, we first analyse the impact of heating rate and storage temperature on T_{cc}.

The impact of heating rate was analysed by using a Fast (F) or a Slow (S) rate at which the oil temperature increases to a constant re-heating oil temperature ($T_{oil,imp}$). After $T_{oil,imp}$ is achieved, it is maintained at a constant level until the end of re-heating. With Fast heating, CCM reaches T_{cc} approximately 1.5-times faster than with Slow heating. These heating types have no significant impact on cold-crystallization temperature, as indicated by similar T_{cc} values of 4-S and 4-F measurements in Fig. 10A. However, larger change in heating rate ought to impact T_{cc}.

Furthermore, heating rate can be increased by elevating $T_{oil,imp}$. This method yields linearly increasing relationship between $T_{oil,imp}$ and T_{cc}, as depicted in Fig. 10A. When heating rate increases, CCM molecules have less time to relax to crystal structure at a certain temperature causing increased T_{cc}. Maintaining a constant $T_{oil,imp}$ in re-heating causes

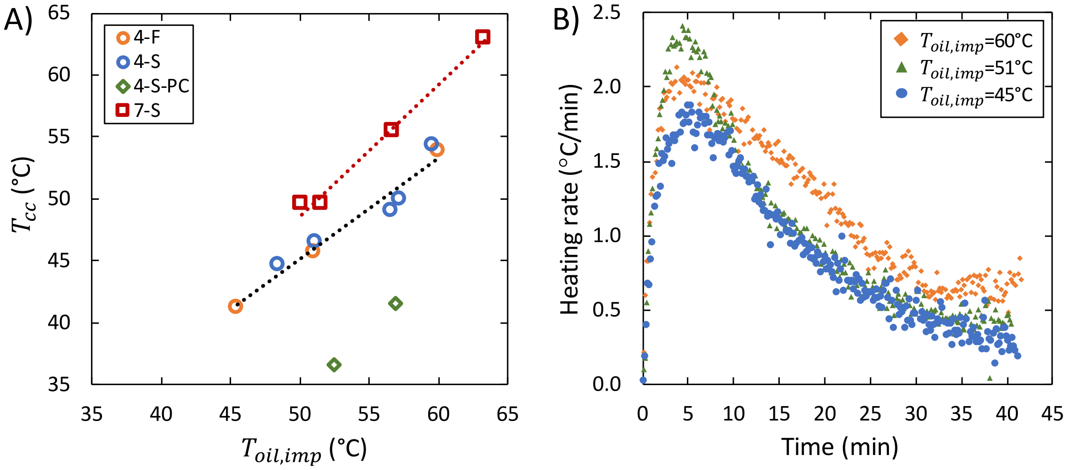

Fig. 10. A) Impact of re-heating oil temperature ($T_{oil,imp}$) to cold-crystallization temperature (T_{cc}). Legend numbers "4″ and "7" refer to storage temperature (4 °C or 7 °C), "F" to fast heating, "S" to slow heating and "PC" to partially crystallized CCM before the measurement. B) Heating rate of 4-F measurements until T_{cc}.

exponentially decreasing heating rate in time. Fig. 10B illustrates the heating rate of CCM as a function of time for three different $T_{oil,imp}$. The heating rate decreases with a reduction of $T_{oil,imp}$, emphasizing the impact of the inlet oil temperature during re-heating.

Fig. 10A also shows that an increase in storage temperature increases T_{cc}. When storage temperature is increased from 4 °C to 7 °C, T_{cc} increases approximately 5 °C. This type of behaviour is expected, as the cooling end temperature, which is in this case the storage temperature, affects the cold-crystallization kinetics. In our previous work, crystallization rate at a constant temperature slowed down significantly, when cooling end temperature was increased from −10 °C to 0 °C [32]. CCM possesses peculiar energy landscape, which most likely causes this behaviour, when material is cooled below 1.2 T_g. Practical applications desire low T_{cc}, because T_{cc} directly correlates to the amount of energy required for re-heating. Therefore, low storage temperature and heating rate are beneficial. However, this contradicts with the practical use, as low storage temperature might require external cooling and slow heating rate reduces the response time. This emphasizes the importance of optimizing the operating conditions for each application separately. For example, the storage unit could be located underground, where the ground temperature naturally maintains at a constant level and sets the boundary for the optimal operating conditions.

In addition, T_{cc} indicates partial crystallization of CCM, by yielding lower values than without premature crystallization (Fig. 10A). Existing crystal phase does not require induction time for crystal formation and new phase can begin to grow on already formed crystal surface area. Reduced T_{cc} was also evident after long-term storage because storage temperatures of 4 °C and 7 °C induced slow crystallization (see Section 3.4). The reduction of T_{cc} depends on the extent of premature crystallization. The design of the experimental setup did not enable determination of the surface area of crystalline phase. Instead, the crystal fractions were estimated from the amount of released heat as 0.15 and 0.11 for T_{cc} of 37 °C and 42 °C in Fig. 10A, respectively. On one hand, low T_{cc} is desired, because re-heating can be completed with less heat at lower temperature. On the other hand, discharged heat is released at lower temperature. For heating purposes, the optimal T_{cc} depends on the temperature level of the application and available heat for re-heating. T_{cc} displayed here (45–60 °C) would be applicable for domestic use, where hot water temperature typically ranges from 30 °C to 60 °C. In addition, district heating systems could benefit from the storage, as low-temperature system supply hot water at approximately 50 °C to 60 °C, and ultra-low systems at 35 °C [35].

3.6. Cold-crystallization – heat release

The heat release of CCM storage units were implemented in two ways. Discharge Type A pumps oil through the storage unit for an entire discharge process. Discharge Type B stops the oil supply when cold-crystallization begins, i.e. when temperature of CCM begins to increase rapidly. Oil pump was turned on again when the cold-crystallization ended, i.e. when the average temperature of CCM peaked. The cold-crystallization and the heat release processes were analysed in Unit 1 in detail, because it provides enhanced heat transfer arrangement between the heat transfer oil and CCM in comparison to Unit 2.

Fig. 11A shows the heat flow in the discharge process of Unit 1 using the two discharge types and the inlet oil temperature of 50 °C. As expected, Type B achieved high maximum discharge rate of ∼ 1000 W, because CCM undergoes complete crystallization before pump was turned on. Therefore, heat transfer from CCM to oil was limiting factor during heat discharge. In the setup, the oil side heat transfer was limited by laminar flow. In larger scale applications, turbulent flow could be achieved at the liquid side, which would further improve the heat transfer rate. Discharge Type A maintained a lower rate for longer time, reaching maximum of ∼ 200 W. In this case, the heat transfer was limited by crystallization kinetics because it occurred slower during the discharge process than compared to Type B. As heat is constantly transferred to the circulating oil, temperature of CCM and oil did not increase to the same level as in Type B. Therefore, crystallization rate or heat transfer within CCM limited Discharge Type A. This caused Discharge type A to consume as much, or even more, time as Type B to complete the discharge, even though the pump was turned off for a while in Type B. These differences in discharging rate and time were evident at low re-heating temperatures ($T_{oil,imp}$), as illustrated in Fig. 11A, where re-heating temperature of $T_{oil,imp}$ = 50 °C was used. When $T_{oil,imp}$ was increased, Discharge Type A also displayed increased discharging rates, as shown in Fig. 11B, where $T_{oil,imp}$ = 60 °C. Discharge Type A was useful, when $T_{oil,imp}$ was approximately 60 °C. At this temperature, CCM's crystallization kinetics was adequately fast to increase outgoing oil temperature to a maximum of approximately 80 °C, which yielded maximum discharging rate of ∼ 500 W. This type of discharging could be useful, for example, in district heating applications, where the returning water is approximately at 60–80 °C, and it could supply the necessary temperature level for re-heating. Otherwise, allowing CCM to crystallize prior heat discharge appears to result in better discharging performance in the heat transfer arrangement of Unit 1. It is noteworthy that the discharging rate forms a peak, first increasing and then decreasing which should be considered in the design of the application.

In comparison, Unit 2 showed only small difference between the discharge types, indicating that the heat transfer from CCM to the oil was limiting factor in both discharging types. Heat transfer could be enhanced by improving heat exchanger configuration, for example by inserting metal fins inside the tubes. Furthermore, discharge rate never reached the same level as in Unit 1. Unit 2 comprised of seven steel tubes, large container and large oil volume, which added to the thermal mass of the unit. The released heat was absorbed by the structure,

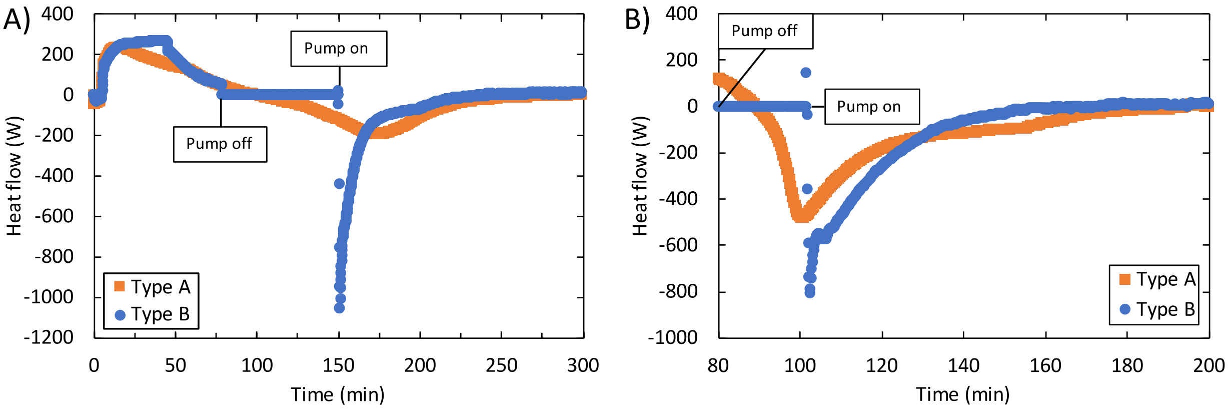

Fig. 11. The heat flow during the discharge Type A and Type B in Unit 1. Re-heating and discharge oil temperature were set to 50 °C (A) and 60 °C (B).

reducing the maximum achievable oil temperature. It would be desirable to reduce structural thermal mass as much as possible, to obtain larger temperature increase of the heat transfer fluid. However, large CCM units are more vulnerable for spontaneous crystallization in cooling, which could lead to premature heat release of a large part of the storage. The supercooling stability was discussed in Section 3.3 Critical cooling rate.

Because re-heating oil temperature impacted the discharging rate, we examined cold-crystallization kinetics of CCM using temperature data from Unit 1 during the crystallization stage of Discharge Type B. In this stage, CCM cold-crystallized without oil circulation, hence the released heat was not transferred away from the unit. For an adiabatic crystallization process with uniform temperature, the crystallized fraction at time t ($\alpha(t)$) can be estimated as the ratio of the temperature increase from the beginning of cold-crystallization (T_{cc}) to T_t and the maximum temperature increase achieved during the crystallization: $\alpha(t) = (T_t - T_{cc})/(T_{max} - T_{cc})$. Moreover, this formulation assumes that the maximum temperature during cold-crystallization (T_{max}) does not achieve the melting temperature (T_m). In this work, heat loss and temperature gradients within the crystallizing CCM reduce the accuracy of the above crystal fraction formulation. We minimized the inaccuracies by applying data only from Unit 1, which had small heat losses and three thermocouples to measure average temperature of CCM. In addition, we analysed four parallel measurements which used Fast cooling mode and 2-day storage period at 4 °C, to minimize the risk of existence of premature crystals. Fig. 12A depicts the development crystal fraction in time for the analysed measurements.

Fig. 12B plots the elapsed time for selected crystallization ranges at different cold-crystallization beginning temperatures (T_{cc}). Maximum crystal fraction of 0.90 was used to minimize the inaccuracy of the measurements at the end of crystallization. As exponential fits indicate, the crystallization time decreases exponentially with an increase in the temperature of CCM, at which the pump was turned off. CCM's crystallization rate constant follows Arrhenius-type temperature dependency from 10 °C to at least 45 °C [32]. As the rate constant is inversely proportional to time, crystallization time ought to show exponential behaviour as well. This behaviour will vanish when melting temperature is approached, because thermodynamic driving force for crystallization decreases, causing crystal growth rate and nucleation rate to decrease. Nevertheless, the exponential form remains valid for the crystallization time in the analysed measurements, implying that the crystallization rate constant follows Arrhenius type temperature dependency throughout the crystallization process. This enables estimation of the crystallization time at different beginning temperatures of crystallization which is beneficial in predicting the response time of the CCM storage. These time predictions apply for a crystallization environment that compares to Unit 1, as numerous metal plates confine crystal growth.

Interestingly, crystallization from $\alpha = 0$ to 0.5 consumes almost as much time as from 0 to 0.9, as illustrated in Fig. 12B. Because the crystallization rate constant follows Arrhenius equation, $\alpha(t)$ shows drastic acceleration towards the end of crystallization (Fig. 12A). Therefore, low re-heating temperatures should be avoided if fast discharge response is desired. In principle, as isothermal cold-crystallization of CCM follows Avrami equation [32], adiabatic cold-crystallization could be modelled by combining Avrami equation and Arrhenius type dependency for the crystallization rate constant. However, this type of detailed modelling would require accurate temperature data for conclusive results, and it was out of the scope of this work.

3.7. *Overall storage performance*

In order to evaluate the overall storage performance of the prototype storage, storage capacity (MJ) and the overall efficiency of the different storage units should be analysed. Fig. 13 depicts a full storage cycle of Unit 1 and Unit 2 in an enthalpy-temperature graph. The difference in charged heat (Q_{chr}) between Unit 1 (~2600 MJ) and Unit 2 (~4700 MJ) evidences the large thermal mass of Unit 2, even though configuration of Unit 1 achieved higher heat transfer area than Unit 2. Naturally, large thermal mass can store more thermal energy, but large volume is required for the storage and the ratio of the latent and sensible heat reduces. Because the stored sensible heat gradually decreases due to heat loss, low thermal mass is desirable. Indeed, the volumetric storage capacities are almost equal: 370 MJ·m^{-3} and 360 MJ·m^{-3} for Unit 1 and Unit 2. These storage capacities were calculated for charging from 4 °C to 128 °C. The overall efficiency of the storage includes the sensible heat of heating and cooling, as formulated in Eq. (5). Q_{ST} refers to the usable heat that is discharged on cooling, i.e., short-term storage. It can be utilized directly, as used in short-term TES, or it can be transferred to a separate short-term storage, such as hot water tank. Q_{LT} refers to the usable heat discharged on cold-crystallization, i.e., heat released after long-term storage. Q_{imp} describes the sensible heat for re-heating the storage from the storage temperature to the cold-crystallization temperature.

$$\varepsilon = \frac{Q_{ST} + Q_{LT}}{Q_{chr} + Q_{imp}} \tag{5}$$

Fig. 13 illustrates the thermal energy involved for each part of the

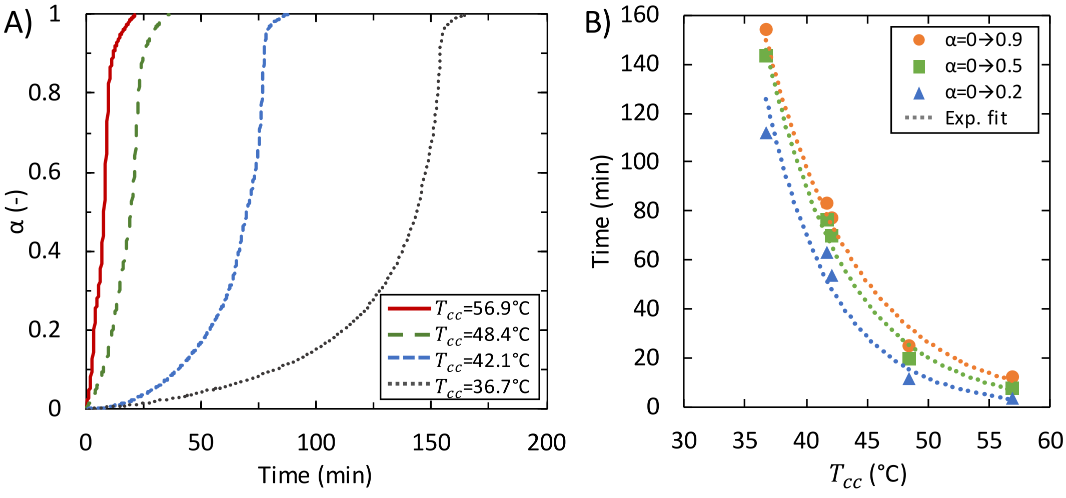

Fig. 12. A) Progress of crystallization (crystal fraction, α) for different beginning temperatures of cold-crystallization. Pump was turned off during cold-crystallization. B) Time for cold-crystallization to reach selected crystal fractions at different beginning temperatures of cold-crystallization with an exponential fit.

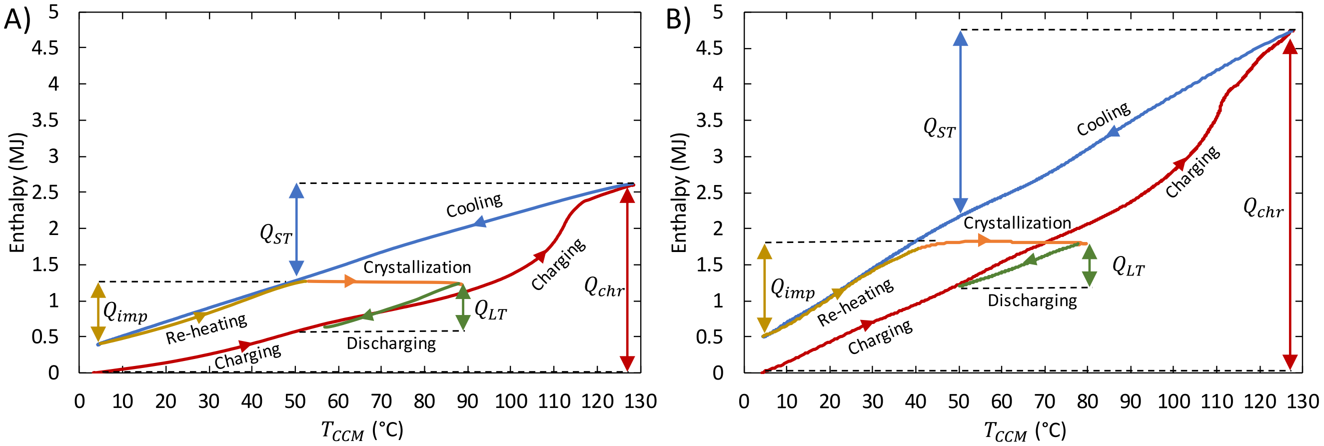

Fig. 13. A complete storage cycle of Unit 1 (A) and Unit 2 (B), when CCM was stored at 4 °C for 2 days. Red colour indicates charging, blue cooling, yellow re-heating, orange cold-crystallization and green discharging. (For interpretation of the references to colour in this figure legend, the reader is referred to the web version of this article.)

storage cycle, when the discharged heat can be used until 50 °C. In this case, Unit 1 (Fig. 13A) yields the overall efficiency of 0.57, which constitutes from the energy release after the short-term storage (0.38) and the long-term storage (0.19). Efficiency of Unit 2 (Fig. 13B), results in 0.52, with short-term share of 0.42 and long-term share of 0.10. The overall efficiencies are similar, but the share of thermal energy released after long-term storage is low for Unit 2. This was caused from the large thermal mass of the unit, which contributes to the sensible storage capacity of the storage. If discharged heat could be utilized until 30 °C, the overall efficiency of Unit 1 increases to 0.77, with short-term share of 0.49 and long-term share of 0.28. Here, the long-term TES share increases, but short-term TES part still dominates the storage capacity. Evidently, short-term storage capacity significantly impacts the efficiency of the storage, but ability to store heat for long-term in parallel to short-term improves the overall efficiency and viability of storing thermal energy. In larger applications, increased share of the long-term storage can be achieved, as increased volumetric ratio of CCM to container (V_{CCM}/V_{cont}) reduces the thermal mass share of the container and heat exchanger. For example, we estimated that the thermal mass of the container and heat exchanger in Unit 1 (~17 % of the total thermal mass) would approach to 7 % of the total thermal mass in larger applications with similar heat exchanger configuration. Above results indicate that the overall efficiency of CCM storage ranges from 0.50 to 0.80, depending on the minimum temperature of the useable heat in the application. For example, domestic hot water is typically used in a temperature range from 30 °C to 60 °C. The long-term storage efficiency was assumed to remain as unity. In reality, heat losses in the pipeline from the storage to the heat demand reduce the amount of usable heat, decreasing efficiency of the storage system.

4. Conclusions

This work confirmed the method of cold-crystallization for reliable long-term storing and release of thermal energy at a kilogram scale for the first time. For this, a prototype TES system determined the operational parameters of using a mixture of erythritol and cross-linked sodium polyacrylate (CCM) for long-term TES. The prototype comprised two storage units with a finned tube heat exchanger (Unit 1) and shell and a closed tube heat exchanger (Unit 2), which were used to analyse each part of the complete storage cycle. Measurements yielded an average melting enthalpy of 166 J/g, which corresponds to the value determined using DSC (178 J/g) within the accuracy of the prototype. The overall efficiency of the storage varied between 0.50 and 0.80, when the latent heat of melting was used for long-term storage and a part of the sensible heat of supercooling for short-term storage. The efficiency was significantly affected by the lowest temperature where the discharged heat was utilized, because the sensible heat of the cooling was larger than the latent heat. For supercooling, we established a critical cooling rate of 0.6 °C/(kg·min) to 0.1 °C/(kg·min) when the temperature of CCM decreased from 100 °C to 20 °C, respectively. Above the critical cooling rate, premature crystallization was not observed in either of the units. Despite this, a momentary heat release rate of 1000 W was achieved by allowing complete cold-crystallization before discharging the heat. The storage efficiency remained high for one month at the storage temperature of 4 °C which corresponds to the storage efficiency measured in 160-g glass bottles in our previous research.

The determined operational parameters in this work demonstrate that reliable supercooling can be achieved with adequate heat release rates during discharging, which is essential because supercooling and cold-crystallization have stochastic nature. The parameters can be used to design larger scale storage system for a given heating application but long- and short-term storage capacity must be carefully considered to ensure efficient operation. The similar supercooling and storage stability in different heat transfer arrangements forwards the use of CCM in applications, as finned heat exchangers can be used to achieve high heat transfer rates without hindering the stability of CCM during the supercooling and the storage stage. The future work should analyse the heat release behaviour in detail and confirm the optimal composition of CCM for real-life applications, where the operation can be evaluated next.

CRediT authorship contribution statement

Konsta Turunen: Conceptualization, Methodology, Validation, Formal analysis, Investigation, Writing – original draft, Writing – review & editing, Visualization, Project administration, Funding acquisition. **Valtteri Mikkola:** Conceptualization, Methodology, Writing – original draft, Formal analysis. **Timo Laukkanen:** Conceptualization, Methodology, Writing – review & editing, Funding acquisition. **Ari Seppälä:** Conceptualization, Methodology, Writing – review & editing, Supervision, Project administration, Funding acquisition.

Declaration of Competing Interest

The authors declare that they have no known competing financial interests or personal relationships that could have appeared to influence the work reported in this paper.

Data availability

Data will be made available on request.

Acknowledgement

This research was funded by Maj and Tor Nessling Foundation, Finland, (201900332); Business Finland (HeatStock-project) and Technology Industries of Finland Centennial Foundation and Jane and Aatos Erkko Foundation, Finland, (Future Makers 2019 Program). The authors wish to acknowledge Prof. Annukka Santasalo-Aarnio for her valuable comments and B.Sc Simon Jech for his contribution in the density measurements.

References

[1] Shamseddine I, Pennec F, Biwole P, Fardoun F. Supercooling of phase change materials: A review. Renew Sustain Energy Rev 2022;158:112172. https://doi.org/10.1016/j.rser.2022.112172.

[2] Hasan Zahir M, Mohamed SA, Saidur R, Al-sulaiman FA. Supercooling of phase-change materials and the techniques used to mitigate the phenomenon. Appl Energy 2019;240:793–817. https://doi.org/10.1016/j.apenergy.2019.02.045.

[3] Sandnes B, Rekstad J. Supercooling salt hydrates: Stored enthalpy as a function of temperature. Sol Energy 2006;80:616–25. https://doi.org/10.1016/J.SOLENER.2004.11.014.

[4] Wang G, Dannemand M, Xu C, Englmair G, Furbo S, Fan J. Thermal characteristics of a long-term heat storage unit with sodium acetate trihydrate. Appl Therm Eng 2021;187:116563. https://doi.org/10.1016/j.applthermaleng.2021.116563.

[5] Safari A, Saidur R, Sulaiman FA, Xu Y, Dong J. A review on supercooling of phase change materials in thermal energy storage systems. Renew Sustain Energy Rev 2017;70:905–19. https://doi.org/10.1016/j.rser.2016.11.272.

[6] Debenedetti PG. Metastable liquids - concepts and principles. New Jersey, USA: Princeton University Press; 1996.

[7] Mullin JW. Crystallization. 4th ed. Oxford: Butterworth-Heinemann; 2001.

[8] Ribezzo A, Falciani G, Bergamasco L, Fasano M, Chiavazzo E. An overview on the use of additives and preparation procedure in phase change materials for thermal energy storage with a focus on long term applications. J Energy Storage 2022;53:105140. https://doi.org/10.1016/j.est.2022.105140.

[9] Ling Z, Luo M, Song J, Zhang W, Zhang Z, Fang X. A fast-heat battery system using the heat released from detonated supercooled phase change materials. Energy 2021;219:119496. https://doi.org/10.1016/j.energy.2020.119496.

[10] Peng S, Hu Y, Huang J, Song M. Surface free energy analysis for stable supercooling of sodium thiosulfate pentahydrate with microcosmic-visualized methods. Sol Energy Mater Sol Cells 2020;208:110390. https://doi.org/10.1016/j.solmat.2019.110390.

[11] Wang H, Zhou G. Experimental investigation on discharging characteristics of supercooled CH3COONa·3H2O-Na2S2O3·5H2O mixtures triggered by local cooling with Peltier effect. Sol Energy 2021;217:263–70. https://doi.org/10.1016/j.solener.2021.02.010.

[12] Tokoro H, Yoshikiyo M, Imoto K, Namai A, Nasu T, Nakagawa K, et al. External stimulation-controllable heat-storage ceramics. Nat Commun 2015;6(1). https://doi.org/10.1038/ncomms8037.

[13] Nakano K, Masuda Y, Daiguji H. Crystallization and melting behavior of erythritol in and around two-dimensional hexagonal mesoporous silica. J Phys Chem C 2015;119:4769–77. https://doi.org/10.1021/jp510048g.

[14] Puupponen S, Mikkola V, Ala-Nissila T, Seppälä A. Novel microstructured polyol–polystyrene composites for seasonal heat storage. Appl Energy 2016;172:96–106. https://doi.org/10.1016/J.APENERGY.2016.03.023.

[15] Hirano S, Takeuchi H. Characteristic of Reheating Operation in Supercooled Thermal Energy Storage Unit for Hot Water Supply or Space Heating. Energy Procedia 2014;57:3140–9. https://doi.org/10.1016/j.egypro.2015.06.060.

[16] Diarce G, Gandarias I, Campos-celador Á, García-romero A, Griesser UJ. Eutectic mixtures of sugar alcohols for thermal energy storage in the 50–90 °C temperature range. Sol Energy Mater Sol Cells 2015;134:215–26. https://doi.org/10.1016/j.solmat.2014.11.050.

[17] Seppälä A, Meriläinen A, Wikström L, Kauranen P. The effect of additives on the speed of the crystallization front of xylitol with various degrees of supercooling. Exp Therm Fluid Sci 2010;34:523–7. https://doi.org/10.1016/j.expthermflusci.2009.11.005.

[18] Duquesne M, Palomo Del Barrio E, Godin A. Nucleation triggering of highly undercooled Xylitol using an air lift reactor for seasonal thermal energy storage. Appl Sci 2019;9(2):267. https://doi.org/10.3390/app9020267.

[19] Delgado M, Navarro M, Lázaro A, Boyer SAE, Peuvrel-Disdier E. Triggering and acceleration of xylitol crystallization by seeding and shearing: Rheo-optical and rheological investigation. Sol Energy Mater Sol Cells 2021;220. doi:10.1016/j.solmat.2020.110840..

[20] Gunasekara SN, Barreneche C, Inés Fernández A, Calderón A, Ravotti R, Ristić A, et al. Thermal energy storage materials (TESMs)—what does it take to make them fly? Crystals 2021;11(11):1276. https://doi.org/10.3390/cryst11111276.

[21] Faraj K, Khaled M, Faraj J, Hachem F, Castelain C. A review on phase change materials for thermal energy storage in buildings: Heating and hybrid applications. J Energy Storage 2021;33:101913. https://doi.org/10.1016/j.est.2020.101913.

[22] Li Z, Lu Y, Huang R, Chang J, Yu X, Jiang R, et al. Applications and technological challenges for heat recovery, storage and utilisation with latent thermal energy storage. Appl Energy 2021;283. https://doi.org/10.1016/j.apenergy.2020.116277.

[23] Peiró G, Gasia J, Miró L, Cabeza LF. Experimental evaluation at pilot plant scale of multiple PCMs (cascaded) vs. single PCM configuration for thermal energy storage. Renew. Energy 2015;83:729–36. https://doi.org/10.1016/j.renene.2015.05.029.

[24] Seppälä A, Turunen K, Yazdani MR. Thermal conductivity of sugar alcohols. Sol Energy Mater Sol Cells 2022;243:111796. https://doi.org/10.1016/j.solmat.2022.111796.

[25] Gil A, Barreneche C, Moreno P, Solé C, Fernández AI, Cabeza LF. Thermal behaviour of D-mannitol when used as PCM: Comparison of results obtained by DSC and in a thermal energy storage unit at pilot plant scale. Appl Energy 2013;111:1107–13. https://doi.org/10.1016/j.apenergy.2013.04.081.

[26] Gunasekara SN, Pan R, Chiu JN, Martin V. Polyols as phase change materials for surplus thermal energy storage. Appl Energy 2016;162:1439–52. https://doi.org/10.1016/j.apenergy.2015.03.064.

[27] Wang G, Xu C, Kong W, Englmair G, Fan J, Wei G, et al. Review on sodium acetate trihydrate in flexible thermal energy storages: Properties, challenges and applications. J Energy Storage 2021;40. https://doi.org/10.1016/j.est.2021.102780.

[28] Xu T, Gunasekara SN, Chiu JN, Palm B, Sawalha S. Thermal behavior of a sodium acetate trihydrate-based PCM: T-history and full-scale tests. Appl Energy 2020;261:114432. https://doi.org/10.1016/j.apenergy.2019.114432.

[29] Puupponen S, Seppälä A. Cold-crystallization of polyelectrolyte absorbed polyol for long-term thermal energy storage. Sol Energy Mater Sol Cells 2018;180:59–66. https://doi.org/10.1016/j.solmat.2018.02.013.

[30] Turunen K, Yazdani MR, Puupponen S, Santasalo-Aarnio A, Seppälä A. Cold-crystallizing erythritol-polyelectrolyte: scaling up reliable long-term heat storage material. Appl Energy 2020;266:114890. https://doi.org/10.1016/j.apenergy.2020.114890.

[31] Yazdani MR, Etula J, Zimmerman JB, Seppälä A. Ionic cross-linked polyvinyl alcohol tunes vitrification and cold-crystallization of sugar alcohol for long-term thermal energy storage. Green Chem 2020;22:5447–62. https://doi.org/10.1039/d0gc01427c.

[32] Turunen K, Yazdani MR, Santasalo-aarnio A, Seppälä A. Exceptional cold-crystallization kinetics of erythritol-polyelectrolyte enables long-term thermal energy storage. Sol Energy Mater Sol Cells 2021;230. https://doi.org/10.1016/j.solmat.2021.111273.

[33] JCGM. Joint Committee for Guides in Metrology. Evaluation of measurement data—Guide to the expression of uncertainty in measurement. JCGM 100 2008.

[34] Pereira J, Eames P. Thermal energy storage for low and medium temperature applications using phase change materials – A review. Appl Energy 2016;177:227–38. https://doi.org/10.1016/j.apenergy.2016.05.097.

[35] Pomianowski MZ, Johra H, Marszal-Pomianowska A, Zhang C. Sustainable and energy-efficient domestic hot water systems: A review. Renew Sustain Energy Rev 2020;128:109900. https://doi.org/10.1016/j.rser.2020.109900.